Electronic Supplementary Material (ESI) for CrystEngComm.
This journal is © The Royal Society of Chemistry 2021

Supporting Information

Reversible facile single-crystal-to-single-crystal polymorphic transition accompanied by unit cell volume expansion and twinning

Kunlin Wang, Chenguang Wang, Manish Kumar Mishra, Victor Young Jr, Changquan Calvin Sun*

List of contents

S1. Materials and methods

1) Single crystal preparation
2) Single crystal structure determination
3) Twinning and composition plane for DPH-CIT Form II
4) Variable temperature unit cell parameters
5) Differential Scanning Calorimetry (DSC)
6) Cryo-Scanning Electron Microscopy (Cryo-SEM)
7) Experimental and calculated Powder X-ray Diffraction data (PXRD)
8) Conformational energy optimization by Gaussian
9) Lattice Energy Calculation
10) Energy Framework calculations

S2. Twinned SCXRD reflection frames of DPH-CIT at 123K

S3. Single crystal unit cell parameters of DPH-CIT forms I and II

S4. Experimental and calculated PXRD traces of DPH-CIT polymorphs

S5. Overlay of DSC and unit cell volume change vs. temperature

S6. Variable temperature unit cell parameters

S7. Torsion angles ϕ1 and ϕ2 in 4 DPH-CIT crystal structures

S8. Supplemental figures on intermolecular interactions and Energy Framework

S9. Figures for Form I single crystal and Form II twinned crystal

S10. Melting point of DPH-CIT form I by DSC

Materials and Methods

1) Single crystal preparation

DPH-CIT (Luxin Pharmaceutical Co., Ltd., Jinan, Shandong, China) was used as received. The single crystal of DPH-CIT was prepared by slow evaporation of a 20 mL isopropyl alcohol solution (5mg/mL) at ambient conditions.

2) Single crystal structure determination

Single crystal X-ray diffraction (SCXRD) of DPH-CIT salt at 148 (2) K and 218 (2) K were performed on a Bruker D8 Venture diffractometer (Bruker AXS Inc., Madison, Wisconsin) equipped with a Bruker PHOTON-II CPAD detector. The data were collected with a MoKα radiation source (IμS 3.0 microfocus sealed tube). Data integration for both 148 (2) K and 218 (2) K was performed with the SAINT program and XPREP was used for space group determination and data merging using the APEX3 software suite. The TWINABS for 148 (K) and SADABS for 218 K programs were used for scaling and absorption correction purposes. The crystal structure was solved and refined using ShelXle program (a graphical user interface for SHELXL[1]). The crystal structure was solved using SHELXT (Intrinsic Phasing) methods. The hydrogen atom bonded to nitrogen was placed as a combination of geometrical placement from the difference Fourier map and refined over least-squares/difference Fourier cycles. Their positions were refined while their thermal parameters were constrained to ride on the carrier atoms. Hydrogen atoms bonded to other atoms were placed in calculated positions, and their positions and thermal parameters were constrained to ride on the carrier atoms. All non-hydrogen atoms were refined with anisotropic displacement parameters. SCXRD structure of DPH-CIT at 123 K was collected on Bruker-AXS Smart Apex-II (Bruker AXS Inc., Madison, Wisconsin) with a MoKα radiation tube source. Data integration for this twinned form was performed with the SAINT program, the TWINABS program was used for scaling and absorption correction purposes and XPREP was used for space group determination and data merging using the APEX3 software suite. Single crystal structure visualization was done using Mercury program,

where the transformation of form II triclinic unit cell to the non-standard setting was done using WinGX for easier comparisons with form I.

3) Twinning and composition plane for DPH-CIT Form II

At temperatures ≤ 148 K the specimen forms a twin by non-merohedry through an enantiotropic phase transition. Form I is found in the monoclinic space group $P2_1/c$ with Z'=1. Form II is found in the triclinic space group P-1 with Z'=2. The two-fold rotation that is part of monoclinic symmetry moves to a pseudo-symmetry relationship between the two independent molecules within the asymmetric unit. This phase transition also requires the two-fold symmetry becomes the twin symmetry element in triclinic symmetry. Indeed, twin indexing indicates a 180° rotation about the *b*-axis that was in Form I. To that end we have adopted the non-standard triclinic setting where the *b*-axis in Form II is aligned with the unique *b*-axis of Form I. This provides for more straightforward illustrations. Composition plane illustrations are presented in Figure S10 by using Mercury (V. 3.10.1, CCDC, Cambridge, UK). In order to build these one needs to fuse two copies of the unit cell contents with respect to the pseudo-symmetry operation found in Form II. This is the 2_1 along the *b*-axis from Form I: (-*x*, *y* + ½, -*z* + ½). The rotational part of this has been supplied by the twin law, as stated above. The translational part of the pseudo-symmetry operation, (0, ½, ½) relates the twin individuals at the composition plane. Therefore, two copies of the asymmetric units are prepared with the second being translated (0, ½, ½) with respect to the first. Finally, these are fused at the *bc* planes. This interface, or layer, has the symmetry of its monoclinic parent.

4) Variable temperature unit cell parameters

Automated fast scans were done using a single crystal of DPH-CIT on a Bruker D8 Venture diffractometer (Bruker AXS Inc., Madison, Wisconsin) equipped with a Bruker PHOTON-II CPAD detector. The data were collected with a MoKα radiation source (IμS 3.0 microfocus sealed tube) from 103K to 298K with different resolutions at different temperature ranges (5K resolution from 118K to 158K;

10K resolution from 158K to 178K, and 30K resolution from 178K to 298K). The unit cell parameters were determined by APEX3 program.

5) Differential Scanning Calorimetry

Differential Scanning Calorimetry (DSC) cycling study was done on a TA instruments Q1000 from -150 ºC (123K) to 25 ºC (298K) at a heating/cooling rate of 10 ºC/min. The instrument was calibrated with indium. Each sample was packed into an aluminum T-zero pan and hermetically sealed with an aluminum lid. The DSC cell was purged with nitrogen gas at 50 mL/min. The coolant used was liquid nitrogen.

6) Cryo-Scanning Electron Microscopy (Cryo-SEM)

DPH-CIT single crystals of different sizes were applied in the Gatan specimen capsule (1.2 mm depth) and placed into a blank cryo-SEM specimen holder. The specimen was transferred from Leica loading station for EM VCT100 to Hitachi UHR FE-SEM SU8230 using Leica EM VCT100 cryo transfer system via Leica EM ACE600. Then, the specimen was cooled to -148° C for SEM analysis using liquid nitrogen. The crystals were evaluated by scanning electron microscopy, operated at SEI mode with an acceleration voltage of 1 kV.

7) Experimental and calculated Powder X-ray Diffraction data (PXRD)

A powder X-ray diffractometer (PANalytical X'pert pro, Westborough, MA) with Cu Kα radiation (1.54059 Å) in the Bragg-Brentano reflection mode was used to characterize DPH-CIT powders at room temperature. Each sample of 10 mg was placed in a metallic sample holder with a flat surface. Samples were scanned at 2θ angles between 5° and 35° with a step size of 0.02° and a collection time of 1 s/step. The simulated PXRD patterns of DPH-CIT forms I and II were obtained from the single crystal structures at 218 and 123 K (CCDC deposition numbers 2012785 and 2012784 respectively) using Mercury (V. 3.10.1, CCDC, Cambridge, UK). The single crystal structure at the transition state 148 K has CCDC deposition number of 2012786.

8) Conformational energy optimization by Gaussian

The cationic DPH molecule was optimized in the gas phase using the Gaussian 16 program[2] at the hybrid functional level of theory B3LYP with 6-31++G(d,p) basis set.[3] The vibrational analysis was performed to ensure convergence of the refinement. The potential energy surface of single DPH cation was scanned in the gas phase with step of 10^{o} by a semi-empirical calculation of PM7, considering the computation speed and accuracy.[4]

9) Lattice energy calculation

The lattice energy of three crystal structures of DPH-CIT obtained at three different temperatures were calculated using the COMPASS force field in the Forcite module (Materials Studio 7.0, Biovia Software Inc., San Diego, CA, USA)[5], with associated charges and ultrafine quality selection. The unit cell parameters were fixed during optimization, while the molecules and crystal packing were allowed to relax, which means the all atom positions were refined. The summation method of 'Ewald' and 'Atom based' were chosen for Electrostatic and van der Waals interactions, respectively. The optimization process reducing the magnitude of calculated forces and (where appropriate) stresses until they become smaller than defined convergence tolerances (energy: 1.0e-4 kcal/mol, force: 0.005 kcal/mol/Å, displacement: 5.0e-5 Å).

10) Energy Framework calculations

The pairwise intermolecular interaction energy was estimated using CrystalExplorer [6] and Gaussian09 [7] with experimental crystal geometry. The hydrogen positions normalized to standard neutron diffraction values were used during the calculation. For each molecule in the asymmetric unit of a crystal, the total intermolecular interaction energy with another molecule, calculated using the CE-B3LYP electron densities model, is the sum of electrostatic, polarization, dispersion, and exchange-repulsion components with scaling factors of 1.057, 0.740, 0.871, and 0.618, respectively [8]. The intermolecular interaction is neglected with molecule–molecule distance more than 3.8 Å.[9]

S2. Twinned SCXRD reflection frames of DPH-CIT at 123 K

Figure S1 depicts two frames of DPH-CIT taken at 123 K and 218 K at the same angle. Compared to the 218 K frame (**Figure S1**a), the frame taken at 123 K shows doubled or split spots at the same positions representing reflections of a twinned crystal (**Figure S1b).**

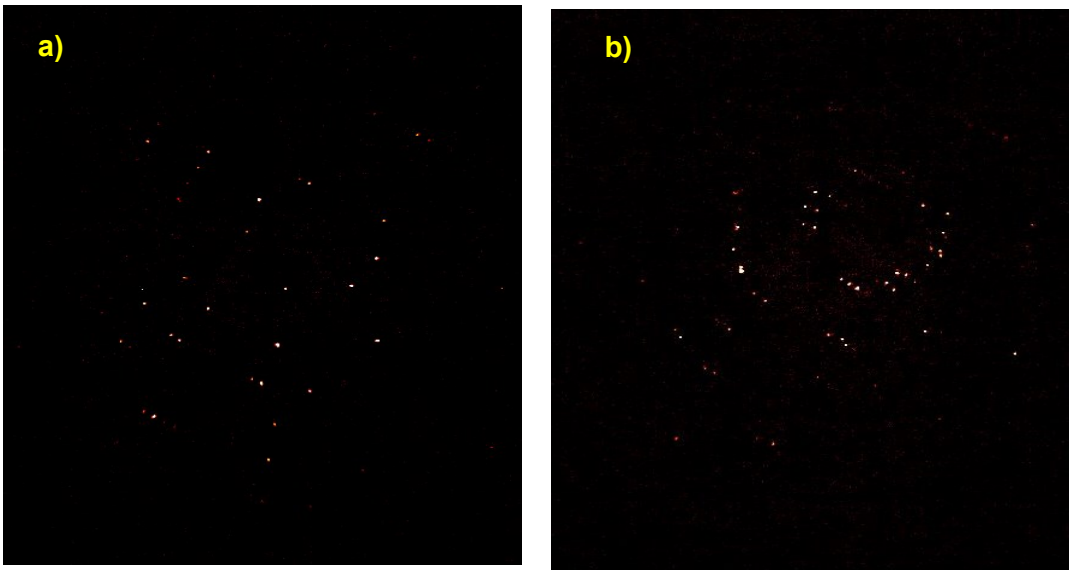

Figure S1. DPH-CIT SCXRD diffraction frame at the same angle at **a)** 218 K and **b)** 123 K

S3. Single crystal unit cell parameters of DPH-CIT forms I and II

Table S1. Unit cell parameters of Forms I and II of DPH-CIT

	Form I	**Transition Phase**	**Form II (twinned)**
Temperature	218 K	148 K	123 K
Crystal system	Monoclinic	Triclinic	Triclinic
Space group	$P2_1/c$	P-1	P-1
Unit cell dimensions	a = 21.229(3) Å b = 9.670(1) Å c = 11.108(1) Å α= 90° β= 91.327(4)° γ = 90°	a = 21.833(19) Å b = 9.359(7) Å c = 11.086(9) Å α= 90.328(17)° β= 92.39(2)° γ = 91.79(2)°	a = 21.893(8) Å b = 9.298(4) Å c = 11.082(4) Å α= 90.070(5)° β= 92.648(5)° γ = 92.006(6)°
Volume	2279.5(4) $Å^3$	2262(3) Å3	2252.0(15) $Å^3$
Z, Z'	4, 1	4, 2	4, 2
Density (calculated)	1.304 Mg/m^3	1.314 Mg/m^3	1.320 Mg/m^3
R factor	0.0427	0.1385	0.0541

S4. Experimental and calculated PXRD patterns of DPH-CIT polymorphs

Figure S2 displays the comparison among experimental and simulated form I and II PXRD patterns of DPH-CIT. The experimental PXRD pattern of DPH-CIT form II cannot be obtained due to lack of cryo-temperature PXRD instrument and the enantiotropic nature of this polymorphic transition.

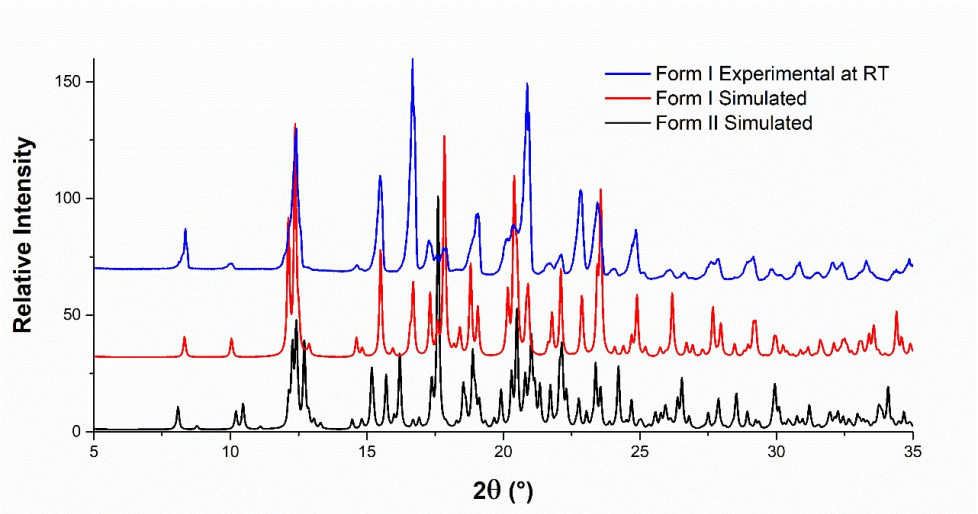

Figure S2. Comparison among PXRD patterns of experimental and simulated forms I (218 K) and II (123 K) DPH-CIT.

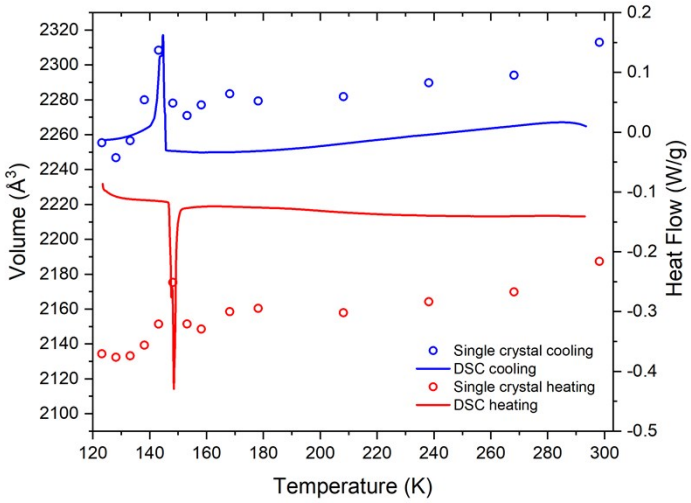

Figure S3. Overlay of DPH-CIT single crystal unit cell volume and DSC curve

S5. Overlay of DSC and unit cell volume change vs. temperature

S6. Variable temperature unit cell angles

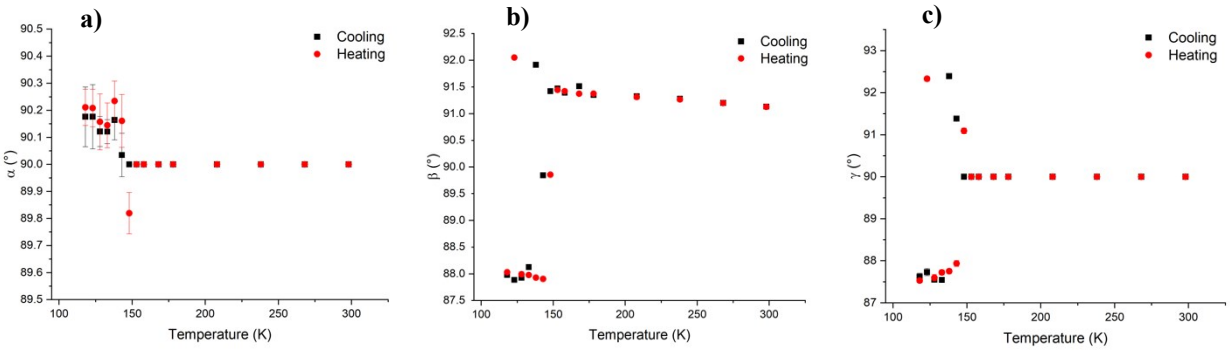

Figure S4. Unit cell angles changes vs. temperature during cooling and heating cycles. **a)** α, **b)** β and **c)** γ. Error bars have been added in all the three graphs.

S7. Torsion angles ϕ1 and ϕ2 in 4 DPH-CIT crystal structures

Table S2. Torsion angles ϕ1 and ϕ2 in 3 DPH-CIT crystal structures; Form II^A and II^B indicates each of the two DPH-CIT salt pair in one asymmetric unit

	Torsion angle	**Angles (°)**
Form I (218K)	**ϕ1** (C13 - C8 - C7 - C6)	-130.94
	ϕ2 (C5 - C6 - C7 - C8)	78.40
Form II^A (148K)	**ϕ1** (C13 - C12 - C4 - C5)	-137.72
	ϕ2 (C12 - C4 - C5 - C16)	55.85
Form II^B (148K)	**ϕ1** (C20 - C21 - C22 - C27)	-90.93
	ϕ2 (C21 - C22 - C27 - C28)	113.84
Form II^A (123K)	**ϕ1** (C13A -C8A - C7A - C6A)	-139.44
	ϕ2 (C8A - C7A - C6A - C5A)	55.89
Form II^B (123K)	**ϕ1** (C12 - C13 - C7 - C6)	-111.31
	ϕ2 (C13 - C7 - C6 - C1)	93.43

S8. Supplemental figures on intermolecular interactions and packing

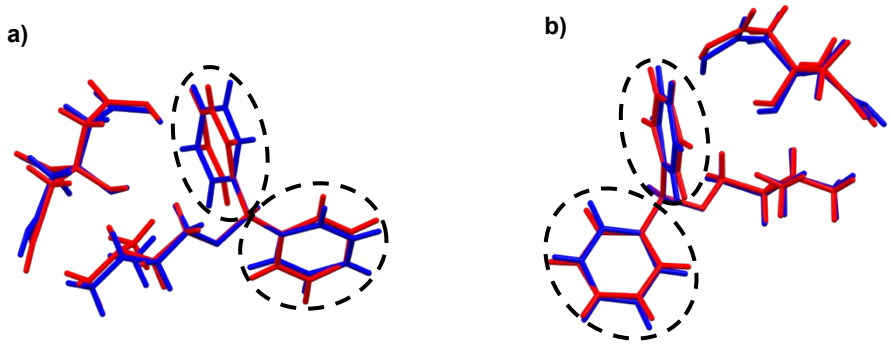

Figure S5. Conformational overlay of asymmetric units of DPH-CIT Form I (red) & **a)** first pair of DPH-CIT in asymmetric unit of Form II at 123 K (II^A, blue), and **b)** second DPH-CIT pair in asymmetric unit of Form II (II^B) at 123 K. These show the different torsion angles in Form I and II as listed in Table 1.

Figure S6. Energy framework representations of (a) Form I (218 K) and (b) Form II (123 K).

Table S3. Intermolecular interaction energies estimated using CE-B3LYP model. Both the total energy (E(tot)) and various components of the energy, i.e., electrostatic (E_{ele}), polarization (E_{pol}), dispersion (E_{dis}), and exchange-repulsion (E_{rep}) are listed. R indicates the distance between centers of mass of the pair of molecules.

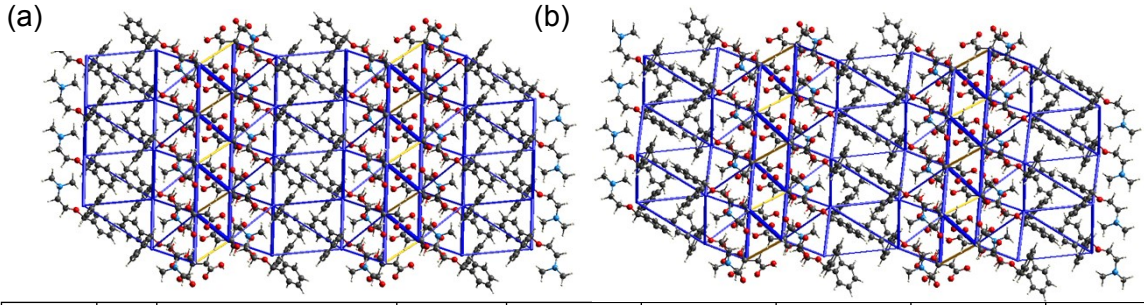

123K	N	Sym operation	R (Å)	E_{ele} (kJ/mol)	E_{pol} (kJ/mol)	E_{dis} (kJ/mol)	E_{rep} (kJ/mol)	E_{tot} (kJ/mol)
	1	-	8.91	87	-4.6	-30.7	23.5	76.3
	1	-x, -y, -z	11.79	80.3	-2	-2.3	0	81.4
	1	-	6.59	191.7	-30	-40.2	22.9	159.6
	1	-	7.81	160.4	-16	-31.9	27.5	146.9
	2	x, y, z	9.26	139.4	-7.1	-11.4	5	135.3
	1	-	6.06	-395	-108.3	-40.1	72.3	-488
	1	-	6.38	-286.1	-56.2	-17.4	17.2	-348.6

	1	-	7.91	161.7	-13.4	-18.9	11.5	151.7
	1	-x, -y, -z	7.85	105.1	-6.3	-16.4	7.8	97
	1	-	6.69	195.6	-30.9	-42.1	21.8	160.8
	1	-	9.33	-156.6	-17.3	-11.1	8.3	-182.9
	1	-	9.85	90.9	-4.4	-19.7	11	82.5
	1	-	9.67	-148.2	-12.3	-7.3	8.3	-167
	1	-	8.27	-235.4	-32.5	-16.2	14.5	-278.1
	1	-x, -y, -z	12.13	90.4	-2.3	-1	0	93.1
	1	-	10.58	-178.2	-13.5	-7.7	2.6	-203.5
	1	-x, -y, -z	13.67	74	-1.3	-1.7	0	75.8
	2	x, y, z	9.26	141.7	-7.5	-12.3	11	140.3
	1	-	8.25	-233.8	-31	-15.3	12.9	-275.6
	1	-x, -y, -z	7.49	104.7	-8.2	-30	16.6	88.8
	1	-	10.69	-174.4	-12.4	-6.4	1.6	-198.1
	1	-	9.56	-151.9	-16.1	-10.2	5.7	-177.9
	1	-	6.74	-289.3	-51.1	-13.9	13.4	-347.5
	1	-	6.26	-398.9	-106.1	-39	70.3	-490.8
	1	-	10	-142.4	-10.7	-6.1	4.6	-161
	1	-	8.25	-233.8	-93.1	-15.3	12.9	-321.5
	1	-	6.38	-286.1	0	-17.4	17.2	-307
	1	-	9.33	-156.6	-16.6	-11.1	8.3	-182.3
	1	-	6.91	69.2	-13.7	-14.9	94.7	108.6
	1	-x, -y, -z	7.06	117.9	-4.5	-4.7	0.2	117.4
	1	-	5.6	50.1	-92.1	-21	174.3	74.3
	1	-	6.26	-398.9	-52.6	-39	70.3	-451.2
	1	-	10	-142.4	-10.7	-6.1	4.6	-161
	1	-	10.58	-178.2	-27.3	-7.7	2.6	-213.7
	1	-	5.48	48.5	-95.9	-22.4	183.7	74.3
	1	-	6.91	64.6	-48.7	-14.3	97.5	80
	1	-x, -y, -z	7.56	126.9	-4.4	-10.3	2.5	123.6
	1	-	9.56	-151.9	-16.1	-10.2	5.7	-177.9
	1	-	6.06	-395	-108.3	-40.1	72.3	-488
	1	-	9.67	-148.2	-12.3	-7.3	8.3	-167
	1	-	8.27	-235.4	-32.5	-16.2	14.5	-278.1
	1	-x, -y, -z	6.99	118.1	-4.6	-5.1	0.3	117.1
	1	-	6.74	-289.3	-51.1	-13.9	13.4	-347.5
	1	-	10.69	-174.4	-12.4	-6.4	1.6	-198.1
	1	-x, -y, -z	7.52	127.4	-4.6	-9.3	2.4	124.6
218K	2	x, -y+1/2, z+1/2	6.56	186.8	-30.6	-45.3	26.3	151.7
	2	x, y, z	9.67	135.8	-6.6	-10.1	6.7	134
	1	-	8.31	-224.6	-27.3	-12.2	8	-263.4
	1	-	10.35	-179.9	-13.7	-7.2	2.2	-205.2
	1	-	9.55	-152.8	-16.6	-11	6.7	-179.2
	1	-x, -y, -z	7.41	106.3	-7.6	-24.6	10.3	91.7
	2	-x, y+1/2, -z+1/2	9.55	89.8	-4.4	-21.4	13.8	81.5

	2	x, -y+1/2, z+1/2	8.31	163	-13.4	-15.9	9.5	154.4
	1	-	6.22	-392.6	-102.9	-37.2	63.3	-484.6
	1	-	6.58	-284.7	-52.6	-15.9	15.6	-344.2
	1	-	9.53	-145.5	-11.9	-7.3	6.9	-164.8
	1	-x, -y, -z	11.07	94.8	-3	-2	0.1	96.3
	2	x, -y+1/2, z+1/2	5.56	49.3	-56.2	-21.2	171.7	98.1
	1	-	6.22	-392.6	-17.3	-37.2	63.3	-421.2
	1	-	9.55	-152.8	-47.6	-11	6.7	-202.2
	1	-	10.35	-179.9	0	-7.2	2.2	-195.1
	1	-	9.53	-145.5	-11.9	-7.3	6.9	-164.8
	1	-	6.58	-284.7	0	-15.9	15.5	-305.3
	1	-x, -y, -z	7.60	125.4	-4.3	-9.6	2.3	122.4
	2	-x, y+1/2, -z+1/2	6.91	66.7	-48	-15	94.1	80.1
	1	-	8.31	-224.6	-4.6	-12.2	8	-246.6
	1	-x, -y, -z	7.14	117.5	-4.4	-4.2	0.1	117.4

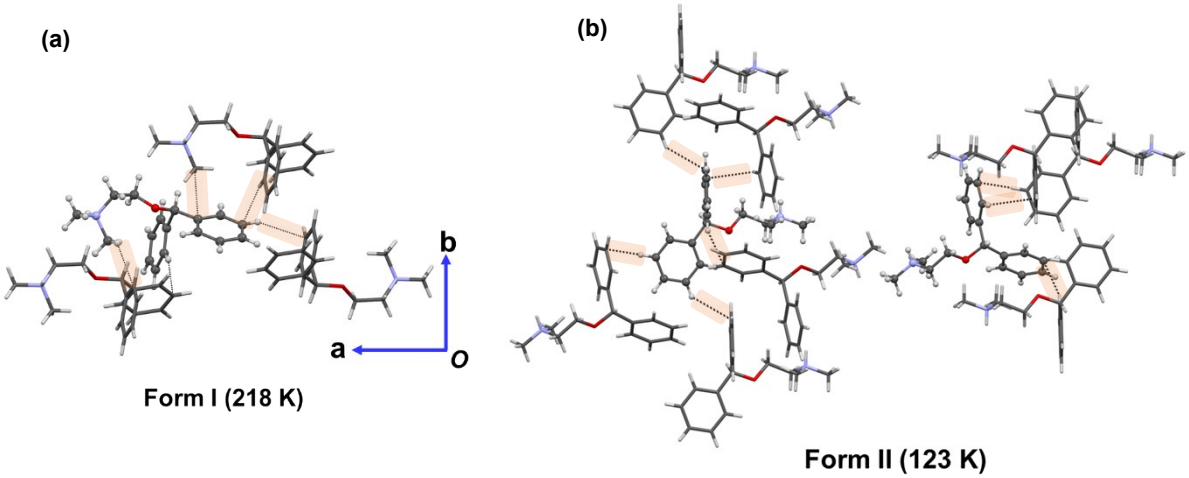

Figure S7. Weak intermolecular C−H···π interactions in Form I (left) and From II (right).

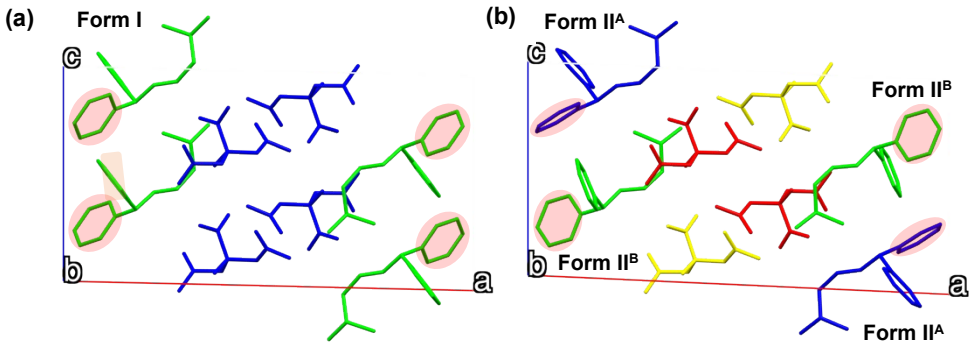

Figure S8. Rotation of phenyl ring helped shorten c-axis length from Form I (218K) in (a) to Form II (100K) in (b) by changing in ϕ1 of Form II^{A}. Hydrogens are omitted for clarity, and the molecules are colored by symmetry.

S9. Figures for Form I single crystal and Form II twinned crystal

The SEM figures of a crystal (**Figure S9**) at room temperature and 123K revealed no change in morphology and surface texture during this SCSC phase transition. The length of crystal along the [001] direction (corresponding to the crystallographic c axis, calculated via BFDH morphology) decreased by 0.007mm due to thermal contraction and phase change.

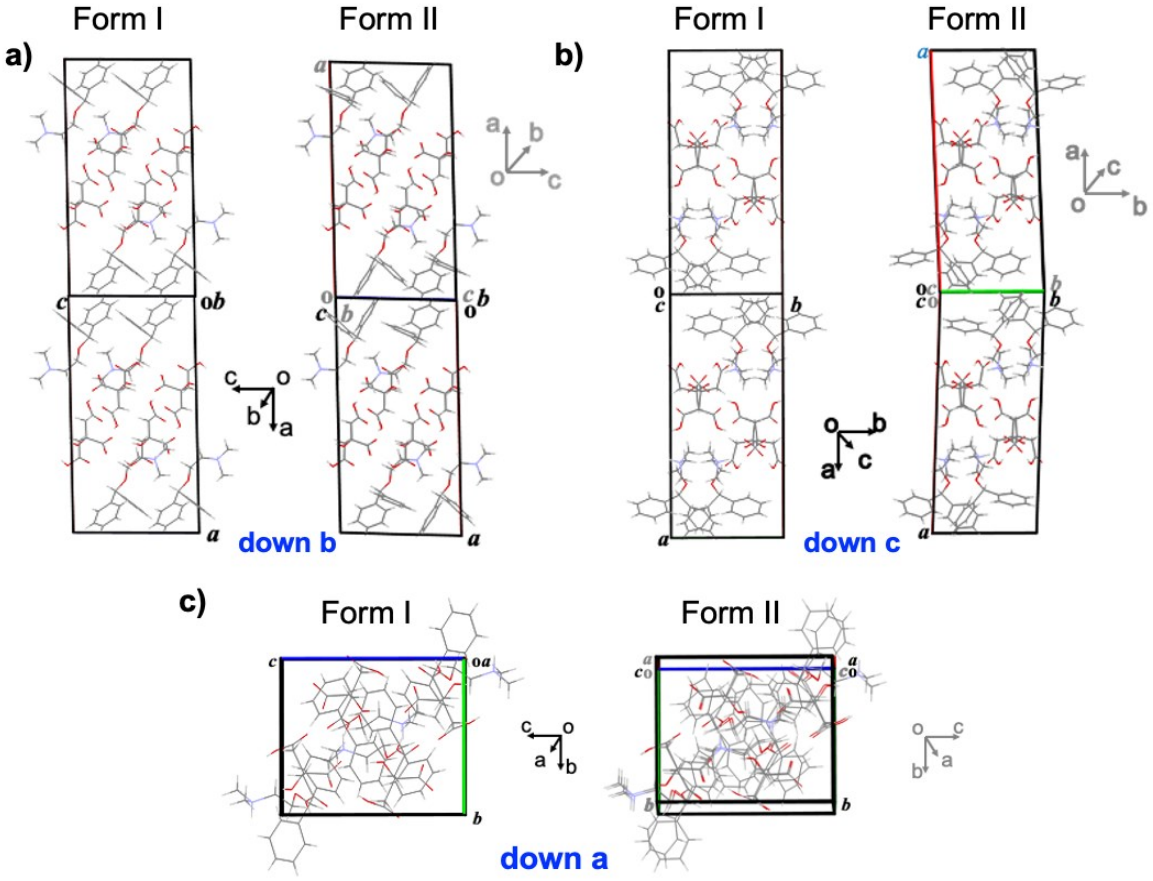

Figure S10. Molecular and unit cell packing illustration of relationship between twinned components of Form II, and comparisons with Form I at 3 different angles: a) Down b axis; b) down c axis and c) down a axis for Form I indicate orientation and the top unit cell for Form I (orientation indicated by the black arrows) I. Grey arrows represent orientations of the twinned component for Form II.

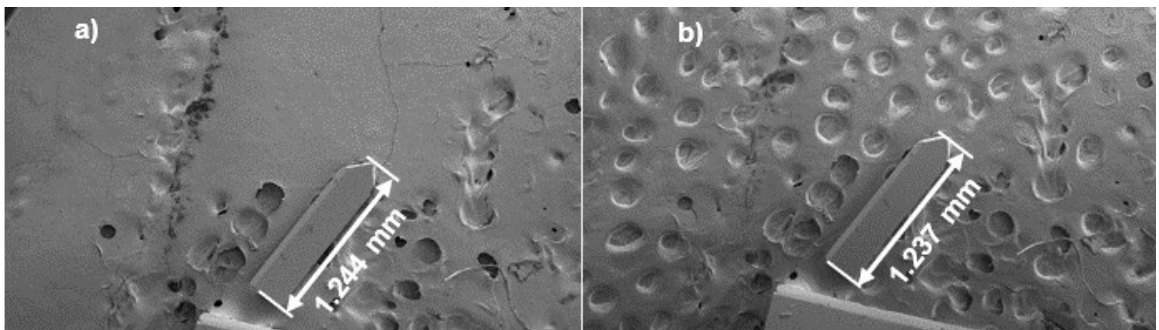

S11. Melting point of DPH-CIT form I by DSC

The melting point of DPH-CIT form I was reported to be 151.3 °C in a previous work. [10]

References

1. Hubschle, C. B.; Sheldrick, G. M.; Dittrich, B. ShelXle: a Qt graphical user interface for SHELXL. *J. Appl. Crystallogr.* **2011,** *44*, (Pt 6), 1281-1284.
2. Frisch, M. J.; Trucks, G. W.; Schlegel, H. B.; Scuseria, G. E.; Robb, M. A.; Cheeseman, J. R.; Scalmani, G.; Barone, V.; Petersson, G. A.; Nakatsuji, H.; Li, X.; Caricato, M.; Marenich, A. V.; Bloino, J.; Janesko, B. G.; Gomperts, R.; Mennucci, B.; Hratchian, H. P.; Ortiz, J. V.; Izmaylov, A. F.; Sonnenberg, J. L.; Williams-Young, D.; Ding, F.; Lipparini, F.; Egidi, F.; Goings, J.; Peng, B.; Petrone, A.; Henderson, T.; Ranasinghe, D.; Zakrzewski, V. G.; Gao, J.; Rega, N.; Zheng, G.; Liang, W.; Hada, M.; Ehara, M.; Toyota, K.; Fukuda, R.; Hasegawa, J.; Ishida, M.; Nakajima, T.; Honda , Y.; Kitao, O.; Nakai, H.; Vreven, T.; Throssel, K.; Jr. Montgomery, J. A.; Peralta, J. E.; Ogliaro, F.; Bearpark, M. J.; Heyd, J. J.; Brothers, E. N.; Kudin, K. N.; Staroverov, V. N.; Keith, T. A.; Kobayashi, R.; Normand, J.; Raghavachari, K.; Rendell, A. P.; Burant, J. C.; Iyengar, S. S.; Tomasi, J.; Cossi, M.; Millam, J. M.; Klene, M.; Adamo, C.; Cammi, R.; Ochterski, J. W.; Martin, R. L.; Morokuma, K.; Farkas, O.; Foresman, J. B.; Fox, D. J. *Gaussian 16*, Revision B.01; Gaussian, Inc.: Wallingford, CT, 2016.
3. Tirado-Rives, J.; Jorgensen, W. L. Performance of B3LYP Density Functional Methods for a Large Set of Organic Molecules. *J. Chem. Theory Comput.* **2008,** *4*, (2), 297-306.
4. Gieseking, R. L. M.; Ratner, M. A.; Schatz, G. C. Benchmarking Semiempirical Methods To Compute Electrochemical Formal Potentials. *J. Phys. Chem. A* **2018,** *122*, (33), 6809-6818.
5. Li, J.; Abramov, Y. A.; Doherty, M. F. New Tricks of the Trade for Crystal Structure Refinement. *ACS Cent. Sci.* **2017,** *3*, (7), 726-733.
6. Turner, M. J.; Wolff, S. K.; Grimwood, D. J.; Spackman, P. R.; Jayatilaka, D.; Spackman, M. A. *CrystalExplorer17*, University of Western Australia: 2017.
7. Frisch, M. J.; Trucks, G. W.; Schlegel, H. B.; Scuseria, G. E.; Robb, M. A.; Cheeseman, J. R.; Scalmani, G.; Barone, V.; Mennucci, B.; Petersson, G. A.; Nakatsuji, H.; Caricato, M.; Li, X.; Hratchian, H. P.; Izmaylov, A. F.; Bloino, J.; Zheng, G.; Sonnenberg, J. L.; Hada, M.; Ehara, M.; Toyota, K.; Fukuda, R.; Hasegawa, J.; Ishida, M.; Nakajima, T.; Honda , Y.; Kitao, O.; Nakai, H.; Vreven, T.; Jr. Montgomery, J. A.; Peralta, J. E.; Ogliaro, F.; Bearpark, M.; Heyd, J. J.; Brothers, E.; Kudin, K. N.; Staroverov, V. N.; Kobayashi, R.; Normand, J.; Raghavachari, K.; Rendell, A.; Burant, J. C.; Iyengar, S. S.; Tomasi, J.; Cossi, M.; Rega, N.; Millam, J. M.; Klene, M.; Knox, J. E.; Cross, J. B.; Bakken, V.; Adamo, C.; Jaramillo, J.; Gomperts, R.; Stratmann, R. E.; Yazyev, O.; Austin, A. J.; Cammi, R.; Pomelli, C.; Ochterski, J. W.; Martin, R. L.; Morokuma, K.; Zakrzewski, V. G.; Voth, G. A.; Salvador, P.; Dannenberg, J. J.; Dapprich, S.; Daniels, A. D.; Farkas, O.; Foresman, J. B.; Ortiz, J. V.; Cioslowski, J.; Fox, D. J. *Gaussian 09*, Revision E.01; Gaussian, Inc.: Wallingford, CT, 2009.
8. Turner, M. J.; Grabowsky, S.; Jayatilaka, D.; Spackman, M. A. Accurate and Efficient Model Energies for Exploring Intermolecular Interactions in Molecular Crystals. *J Phys Chem Lett* **2014,** *5*, (24), 4249-55.
9. Turner, M. J.; Thomas, S. P.; Shi, M. W.; Jayatilaka, D.; Spackman, M. A. Energy frameworks: insights into interaction anisotropy and the mechanical properties of molecular crystals. *Chem. Commun.* **2015,** *51*, (18), 3735-8.
10. Wang, C. G.; Paul, S.; Wang, K. L.; Hu, S. Y.; Sun, C. Q. C. Relationships among Crystal Structures, Mechanical Properties, and Tableting Performance Probed Using Four Salts of Diphenhydramine. *Cryst. Growth Des.* **2017,** *17*, (11), 6030-6040.